Received: 31 January 2024 | Revised: 30 March 2024 | Accepted: 10 April 2024

DOI: 10.1111/sapm.12697

STUDIES IN APPLIED MATHEMATICS WILEY

SPECIAL ISSUE ARTICLE

Modelling Wave Propagation: Mathematical Theory and Numerical Analysis, in Memory of V. Dougalis

From primary HPV infection to carcinoma in situ: A mathematical approach to cervical intraepithelial neoplasia

Vasiliki Bitsouni[1] | **Nikolaos Gialelis**[2,3] | **Ioannis G. Stratis**[2] | **Vasilis Tsilidis**[1]

[1]Department of Mathematics, University of Patras, Patras, Greece

[2]Department of Mathematics, National and Kapodistrian University of Athens, Athens, Greece

[3]School of Medicine, National and Kapodistrian University of Athens, Athens, Greece

Correspondence
Vasiliki Bitsouni, Department of Mathematics, University of Patras, GR-26504 Rio, Patras, Greece.
Email: vbitsouni@math.upatras.gr

Abstract

Cervical intraepithelial neoplasia (CIN) is the development of abnormal cells on the surface of the cervix, caused by a human papillomavirus (HPV) infection. Although in most of the cases it is resolved by the immune system, a small percentage of people might develop a more serious CIN which, if left untreated, can develop into cervical cancer. Cervical cancer is the fourth most common cancer in women globally, for which the World Health Organization (WHO) recently adopted the Global Strategy for cervical cancer elimination by 2030. With this research topic being more imperative than ever, in this paper, we develop a nonlinear mathematical model describing the CIN progression. The model consists of partial differential equations describing the dynamics of epithelial, dysplastic, and immune cells, as well as the dynamics of viral particles. We use our model to explore numerically three important factors of dysplasia progression, namely, the geometry of the cervix, the strength of the immune response, and the frequency of viral exposure.

KEYWORDS
basement membrane, cervical cancer, cervical intraepithelial neoplasia (CIN), human papillomavirus (HPV), mathematical modeling, numerical simulation, precancerous lesions

1 | INTRODUCTION

Healthy cells multiply and die in an orderly way, so that each new replaces one lost. However, if a cell is damaged, for example, due to a virus infection that the immune system failed to defeat, the new damaged cells will either die or start to proliferate in an uncontrolled manner, creating a signaling of oncogenes that act by mimicking growth signaling.[1] The alterations in signal pathways, which can impact the cell's normal biological behavior, include changes such as excessive proliferation, resistance to apoptosis, and evasion of an immune response, leading to the development of an abnormal mass of tissue that differs in clinically important phenotypic features: the tumor.[2] The most common cancers develop from the skin, breast, endometrium, prostate, colon, lung, pancreas, bladder, liver, and cervix.[3] Organs and blood vessels throughout the body are covered by a protective layer of compactly packed cells with a little intercellular matrix, the epithelium or epithelial tissue. These cells, known as epithelial cells, may undergo the aforementioned abnormality which may result in cancer.

A key role in cancer growth, as well as diagnosis and treatment,[4] is played by the immune system, a complex network of organs, cells, and proteins that defends the body against infection that bacteria, viruses, fungi, or parasites can cause while protecting the body's own cells. It is a collection of reactions and responses that the body makes to damaged cells or infections. So, it is sometimes called the immune response. The immune system is important to people with cancer because: (i) cancer can weaken the immune system; (ii) cancer treatments might weaken the immune system; and (iii) the immune system may help to fight cancer.

Cervical cancer is the fourth most common cancer in women globally with an estimated 604000 new cases and 342000 deaths in 2020,[5] representing nearly 8% of all female cancer deaths every year.[6] About 90% of these deaths caused by cervical cancer occurred in low- and middle-income countries with sub-Saharan Africa (SSA), Central America, and South-East Asia having the highest rates of cervical cancer incidence and mortality.[5]

World Health Organization (WHO) has classified the premalignant lesions mild, moderate, or severe dysplasia or carcinoma in situ (CIS).[7] Carcinoma in situ, also known as stage 0 cancer or "in situ neoplasm," is the stage at which a group of abnormal cells in an area of the body appears. The cells may develop into cancer at some time in the future. The changes in the cells are called dysplasia and at this stage the number of abnormal cells is too small to form a tumor. These cell changes, also known as "precancerous changes" or "noninvasive cancer," may not develop into cancer, and usually the CIS is too small to show up on a scan.

In order to emphasize the spectrum of abnormality in these lesions, and to help standardize treatment, the term cervical intraepithelial neoplasia (CIN) was developed.[8] For premalignant dysplastic changes, cervical intraepithelial neoplasia grading (CIN1–3) is used, classifying mild dysplasia as CIN1, moderate dysplasia as CIN2, and severe dysplasia and CIS as CIN3.[9] Histologically, the epithelial tumors of the uterine cervix can be classified into squamous cell carcinoma (SCC), glandular tumors and precursors, mesenchymal tumors and tumor-like conditions, mixed epithelial and mesenchymal tumors, melanocytic tumors, miscellaneous tumors, lymphoid and

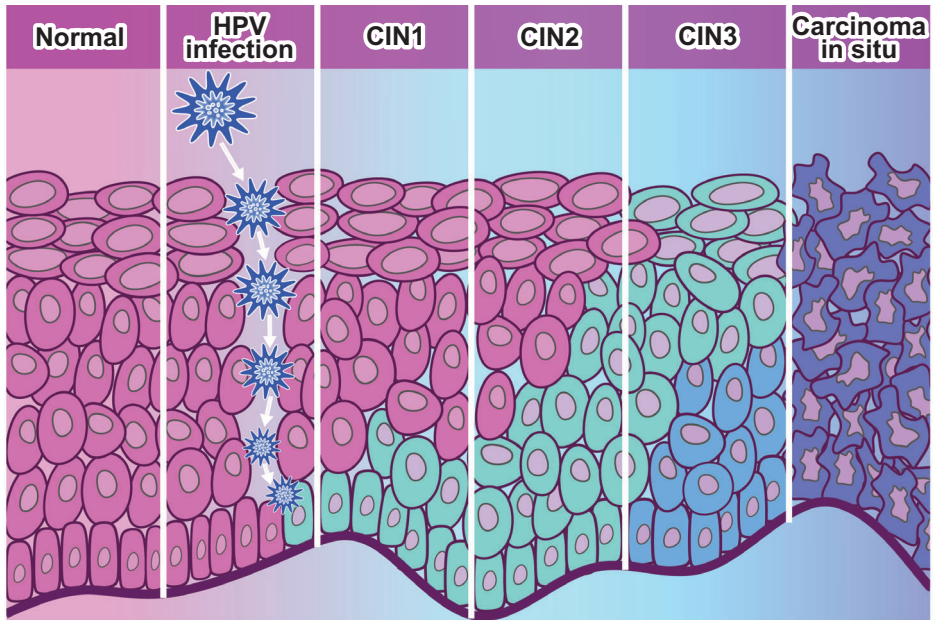

FIGURE 1 Cervical precancerous lesions classification based on the CIN (cervical intraepithelial neoplasia) staging. These lesions are initiated with human papillomavirus (HPV) infection. HPV viral particles traverse the epithelium, infecting the cells of the basal layer.

hematopoietic tumors, and secondary tumors.[10] From the aforementioned types of cervical cancers, the most commonly reported are SCC (75%) and adenocarcinoma, a type of the glandular tumor and precursors (25%).

It has been reported that approximately 95% of cervical cancer cases are caused by persistent genital high-risk human papillomavirus (HPV) infection.[11–14] HPV is a common sexually transmitted infection (STI), which can affect the skin, genital area, and throat.[15,16] All sexually active people have been susceptible to the infections once in a lifetime, regardless of gender, genetic background, and geographical location. A total of 90% of the cases are being resolved with no symptoms within 2 years,[5] whereas in some cases, the infection persists and results in either warts or precancerous lesions.[17] There are nearly 200 types of HPV.[18] Types 16 (reported as the most carcinogenic and associated with more than 60% of cervical squamous cancers and adenocarcinomas[19]) and 18 (more commonly associated with cervical squamous cancers and adenocarcinomas, and together with type 45 cause approximately 20% of cancers[19]) are referred to as high risk and are being detected in more than 90% of cervical cancer lesions.[20]

The life cycle of HPV is strongly linked to the differentiation state of the host epithelial cell and is governed by the action of both viral and cellular proteins.[21,22] First, the virus accesses the basal epithelial cells in the cervix of a woman through microlesions (see Figure 1). By entering these basal cells of the squamous epithelium, the virus establishes the viral cycle. Then, through bindings the viral material manages to enter into the nucleus, where the virus deploys the host cell replication machinery and starts viral genomic replication at about 50–200 copies per cell.[23,24] The infected cells either remain persistently infected until they become cleared by the immune response or progress to cancers. In particular, the infected cells express viral proteins interacting with the normal cell cycle, promoting proliferation and deactivating certain tumor suppressor proteins.[25] It follows a viral genome replication and cell division that would lead in migration of

the daughter cells from the basal layer to the other layers, as well as an uncontrolled proliferation of the HPV-infected cells.[26]

Since the 1920s when the Papanicolaou test (also referred to as Pap test, Pap smear, cervical smear, and cervical screening) was introduced by the Greek physician George N. Papanicolaou as a cervical screening method used to detect potentially precancerous and cancerous processes in the cervix, there has been ongoing research not only for the detection, but most importantly for the prevention of HPV infection and as a consequence of cervical cancer. Tests used in cancer screening programs can pick up carcinomas in situ in the cervix. In fact, a very recent cervical screening self-test is being introduced in more and more countries within the Global Strategy for cervical cancer elimination by 2030,[27] which proposes global vaccination, screening, and treatment. As for the prevention, the first HPV vaccine became available in 2006 and since then 125 countries include HPV vaccines in their routine vaccinations for girls, and 47 countries also for boys.[28] Currently, there are six licensed HPV vaccines, which are highly efficacious in preventing infection with virus types 16 and 18.[29] Prophylactic vaccination against HPV, screening, and treatment of precancer lesions are effective ways to prevent cervical cancer and are very cost-effective. If cervical cancer is diagnosed at an early stage and treated promptly it can be cured. However, the first step to be taken is to understand the mechanism between the HPV infection and cervical cancer progression depending on the (i) viral load, (ii) geometry of the domain under examination, and (iii) immune response.

To the authors' best knowledge, the literature about precancerous lesions that lead to CIS is poor (see, e.g., Refs. 30, 31). The early mathematical models on cervical cancer were focused on epidemiology, describing the transmission dynamics between individuals and the impact of the HPV vaccine (see, e.g., Refs. 32–39 and many references therein). There are only a few later examples of mathematical models for the dynamics of HPV-infected cells at the molecular or tissue levels, such as the models in Refs. 25, 40, which were focused on the progression of cervical cells from normal cells into precancerous and cancerous classes.

In the present work, a continuum mechanical model is introduced in order to describe the spatiotemporal dynamics of the cervical epithelial cells, HPV viral particles, dysplastic and immune cells, and the CIN progression is studied as a result of their interaction. The focus of this work is given to certain, key—as it is established here—factors of the dysplasia progression, such as the geometry of the basement membrane, the strength of the immune response, and the frequency of viral exposure. To this end, various scenarios will be studied and 3D numerical simulations will be run in order to reproduce the patterns widely accepted by the medical community concerning the staging of the lesions.

The layout of this paper is as follows. In Section 2, we formulate a novel model of nonlinear partial differential equations for the dynamics of the epithelial, dysplastic, and immune cells, as well as the viral particles. In Section 3, we numerically investigate certain key factors of dysplasia progression. We conclude in Section 4 with a summary and discussion of the results.

2 | MODEL FORMULATION

In this section, we develop the spatial and dynamical parts of our model.

2.1 | Histology and spatial structure

The vaginal epithelium is a type of stratified squamous epithelium that lines the vagina. It plays a significant role in protecting the body from pathogens. The endocervix epithelium is a type of

columnar epithelium that lines the endocervix. The transitional area between the two aforementioned epithelia is called squamocolumnar junction. This area is susceptible to HPV infection and is the region where physiological transformation to squamous metaplasia occurs.[41]

Epithelial tissue proliferates or regrows through a process called epithelialization. During epithelialization, epithelial cells, especially keratinocytes, proliferate in the basal layer, differentiate as they rise through the spinous and granular layer, and then lose their nucleus and flatten to become the outer layer of skin known as the *stratum corneum*.[42]

Hence, we can differentiate the vaginal epithelium into two layers, based on whether the epithelial cells of that layer are proliferating or not; the proliferative layer and the nonproliferative layer.

2.1.1 | Proliferative layer

The proliferative layer consists of the basal cells which are supported by the basement membrane.

Basement membrane

The basement membrane is a specialized extracellular matrix structure that separates the epithelium from the underlying connective tissue. It is a thin, pliable sheet-like structure, with its primary function being to anchor the epithelium to the underlying connective tissue. It also provides physical and structural support to the epithelium.[43,44]

The shape of the basement membrane is wave-like with neither a specific spatial frequency nor amplitude throughout the tissue, as can be observed from various histological images (see Refs. 45, 46 and references therein). Hence, in order to investigate how its shape affects the formation of dysplastic cells, we have to be able to generate a wide range of different basement membrane shapes. We will model the basement membrane as a surface, due to it being very thin.

There are many ways to generate a random surface.[47] Due to the wave-like shape of the basement membrane, we will use the method presented in Ref. 48, as it utilizes the Fourier series—a natural way to describe wave phenomena. Thus, according to Ref. 48, a random 3D surface can be expressed as:

$$f(x,y)=\sum_{m=-M}^{M}\sum_{n=-N}^{N}a(m,n)\cos((2\pi x,2\pi y)\cdot\boldsymbol{\nu}-\phi(m,n)),$$

where for the (m,n) th term of the Fourier series: $a(m,n)$ is its *amplitude*, $\boldsymbol{\nu}$ is its *spatial frequency*, and $\phi(m,n)$ is its *phase angle*.

Regarding $\boldsymbol{\nu}$, we allow for a discrete set of spatial frequencies:

$$\boldsymbol{\nu}=(m,n),\ \text{for}\ (m,n)\in\left\{(m,n)\in\mathbb{Z}^2|(m,n)\in[-M,M]\times[-N,N]\right\}.$$

Regarding ϕ, we assume that each phase angle follows a uniform distribution on the 2D set $\left[-\frac{\pi}{2},\frac{\pi}{2}\right]^2$:

$$\phi\sim\mathcal{U}\left(\left[-\frac{\pi}{2},\frac{\pi}{2}\right]^2\right).$$

Regarding a, because slower oscillations are more likely to have a larger amplitude than faster ones, we have to reduce the amplitude of the terms of the Fourier series which have high frequency:

$$a(m,n) = a_c(m,n)\ell(m,n),$$

with

$$a_c(m,n) = \begin{cases} 0, & \text{for } (m,n) = \mathbf{0}_2, \\ \|\boldsymbol{\nu}\|^{-\beta} = \left(m^2+n^2\right)^{-\frac{\beta}{2}}, & \text{otherwise,} \end{cases}$$

where $\beta \in \mathbb{R}$ is called the *spectral exponent* and indicates how quickly higher frequencies are attenuated, whereas ℓ follows the standard 2D normal distribution:

$$\ell \sim \mathcal{N}_2(\mathbf{0}_2, \boldsymbol{I}_2),$$

where $\mathbf{0}_2$ is the zero vector of $\mathbb{R}^2$ and $\boldsymbol{I}_2$ is the identity matrix of $\mathbb{R}^{2\times 2}$. If the spectral exponent is large (respectively, small), higher frequencies will (respectively, not) be attenuated, thus making the surface smoother (respectively, rougher).

Therefore, the basement membrane is approximated by

$$f(x,y) = \sum_{m=-M}^{M} \sum_{n=-N}^{N} a_c(m,n)\ell(m,n)\cos(2\pi(xm+yn) - \phi(m,n)).$$

Figure 2 depicts different basement membranes for different values of β and different samples of ℓ and ϕ.

Basal layer

The basal layer, also known as *stratum basale*, is the innermost layer of the epidermis. This layer plays a crucial role in cell replacement and differentiation. It is the layer from which new cells are derived and it is constantly dividing to replace old, damaged cells in the epidermis.[43]

We have already seen how to approach the construction of the basement membrane, f, as a random 3D surface, but how about the basal layer? This time, things should be specific and not random. In fact, we can rely on certain ubiquitous laws in order to determine the basal layer's geometry.

Considering that the basal layer lies on a flat basement membrane, f_0, then, under the hypothesis that the density is everywhere constant, we expect that the width of the layer, h, is also everywhere constant, say h_0, and the upper boundary of the layer, g, is also a flat graph of constant amplitude, $g_0 = f_0 + h_0$. In case where f is not constant, a transition between those two cases, which is depicted in Figure 3, should obey the law of conservation of mass, m. Hence,

$$\underset{\substack{\text{arbitrary part of}\\ \text{basal layer}\\ \text{in first case}}}{\int} dm_0 = \underset{\substack{\text{same part of}\\ \text{basal layer}\\ \text{in second case}}}{\int} dm,$$

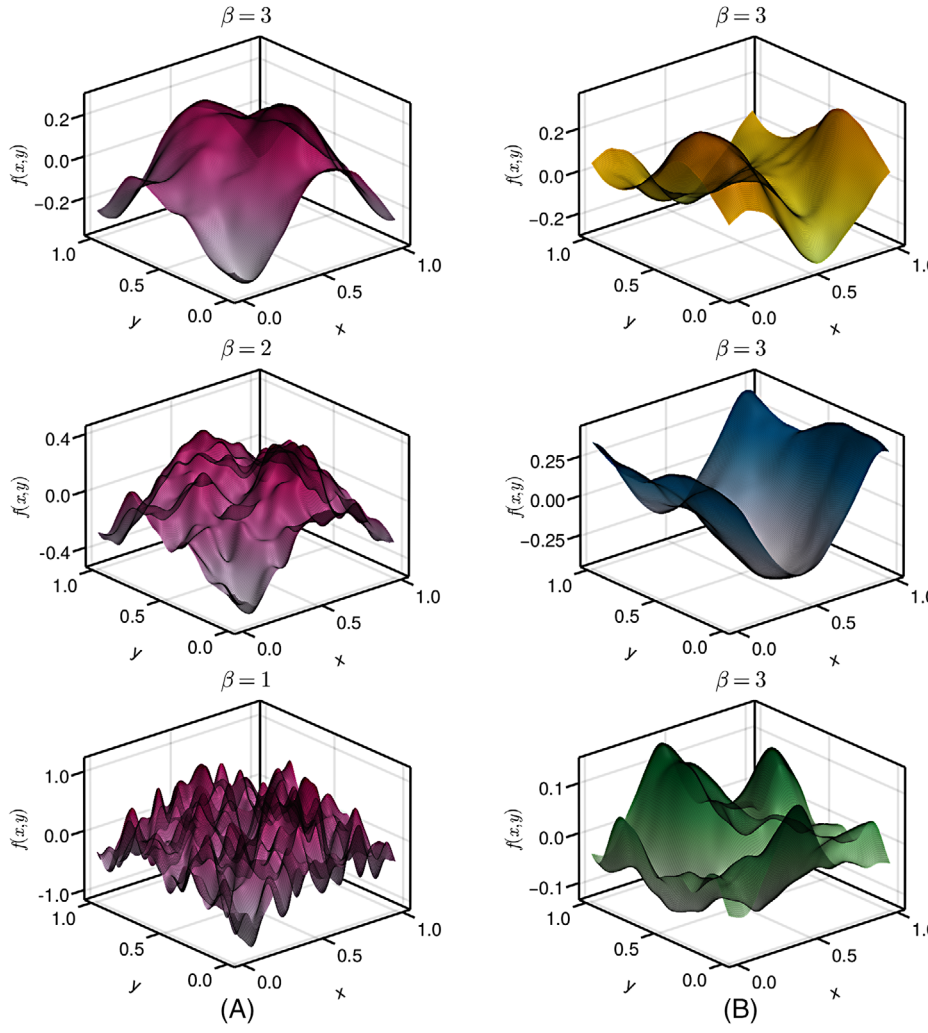

FIGURE 2 The graph of f for random samples of ℓ and ϕ, with (A) different values of β, and (B) the same value of β. The different colors represent different pairs of ℓ and ϕ. In addition, we have that $N = M = 10$.

thus

$$\varpi_0 \int_{\substack{\text{arbitrary part of}\\ \text{basal layer}\\ \text{in first case}}} dV_0 = \varpi_0 \int_{\substack{\text{same part of}\\ \text{basal layer}\\ \text{in second case}}} dV,$$

where ϖ and V stand for the density and the volume, respectively, of the layer, or else

$$h_0 \int_{\substack{\text{arbitrary part of}\\ \text{basement membrane}\\ \text{in first case}}} d\sigma_0 = \int_{\substack{\text{same part of}\\ \text{basement membrane}\\ \text{in second case}}} h d\sigma,$$

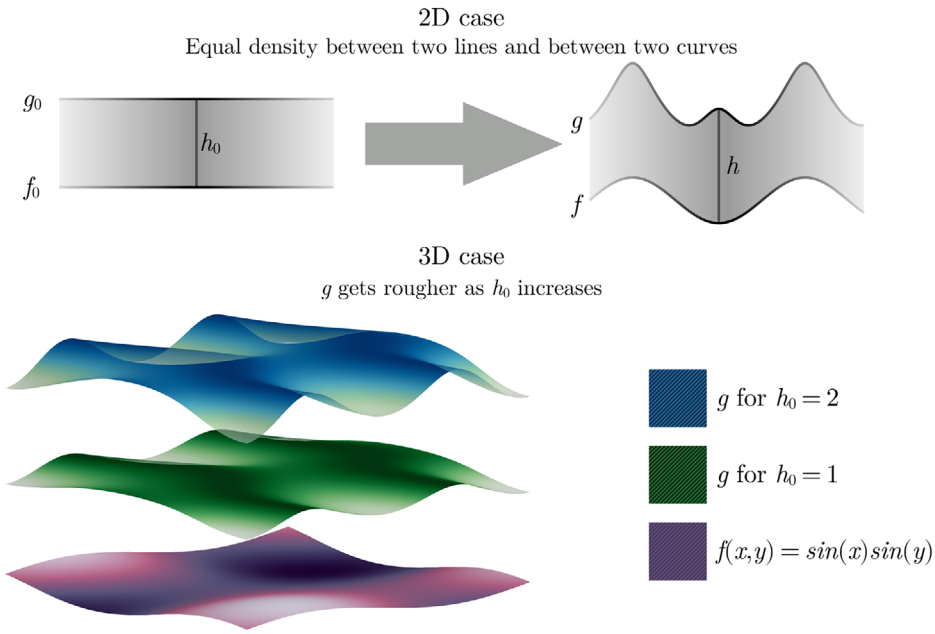

FIGURE 3 Vertical illustration of the geometry of the basal layer.

where σ stands for the surface area of the membrane f. Taking into consideration the geometry of the problem, we deduce that

$$h_0 \iint_D dxdy = \iint_D h\sqrt{1 + \left(\frac{\partial f}{\partial x}\right)^2 + \left(\frac{\partial f}{\partial y}\right)^2}\, dxdy,$$

or else

$$h_0 = \iint_D h\sqrt{1 + \left(\frac{\partial f}{\partial x}\right)^2 + \left(\frac{\partial f}{\partial y}\right)^2}\, dxdy,$$

where $D \subseteq \mathbb{R}^2$ is an arbitrary nontrivial open subset of the domain of f. Now letting $|D| \to 0$, we get from the Lebesgue–Besicovitch differentiation theorem that

$$h = \frac{h_0}{\sqrt{1 + \left(\frac{\partial f}{\partial x}\right)^2 + \left(\frac{\partial f}{\partial y}\right)^2}},$$

therefore

$$g = f + \frac{h_0}{\sqrt{1 + \left(\frac{\partial f}{\partial x}\right)^2 + \left(\frac{\partial f}{\partial y}\right)^2}}.$$

Henceforward, we write Ω_3 for the basal layer, which lies between the surfaces f and g.

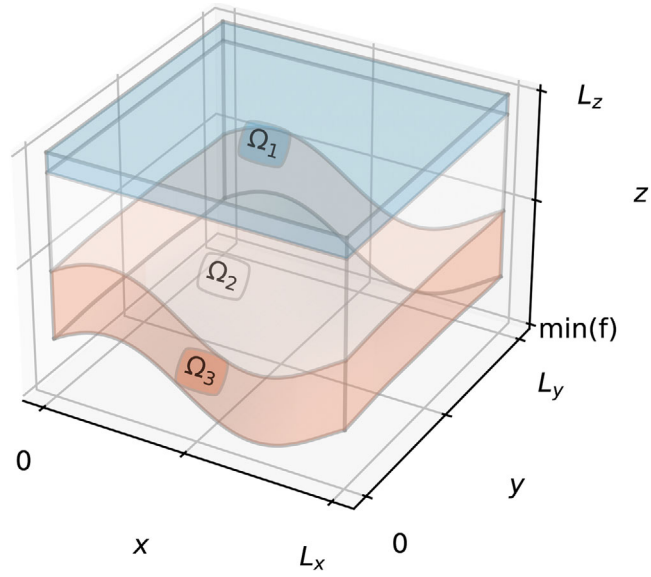

FIGURE 4 The domain, Ω, of the proposed model.

2.1.2 | Nonproliferative layer

Nonproliferative layer is composed of stratified squamous cells and consists of four sublayers: the *stratum granulosum*, *stratum spinosum*, *stratum lucidum*, and *stratum corneum*. Each layer plays a specific role in the epithelium's function and is the result of the squamous cell differentiation program. For example, after a slow coordinated process in space and time, the *stratum corneum* is formulated by a layer of dead cells (corneocytes) to create a physical barrier for the skin.

Henceforth, we write Ω_2 for the nonproliferative layer, which lies on top of Ω_3.

2.1.3 | Unified domain

For modeling needs, we consider Ω_1 to be an additional layer above Ω_2, in order to incorporate the external environment of the epidermis. Moreover, Ω stands for the union of the three layers, Ω_1, Ω_2, and Ω_3, along with their boundaries, and is presented in Figure 4. Moreover, L_x and L_y are the lengths of Ω in the respective horizontal axes, and L_z is the lowest admissible value of the length of Ω in the vertical axis. We assume the width of Ω_1 to be 10% of L_z.

2.2 | Pathology and dynamics

In this section, we describe the key features of the pathology regarding the proliferation of dysplastic cells, along with their interactions with epithelial cells, HPV viral particles, and immune cells. We use u to symbolize the concentration of epithelial cells, v for the concentration of HPV viral particles, c for the concentration of dysplastic cells, and w for the concentration of immune cells.

2.2.1 | Epithelial cells

We begin by assuming that epithelial cells proliferate in a constant manner. The proliferative part of the epithelium is the basal one.[43] Therefore, we assume that the constant proliferation term of the epithelial cell population, s_u to have the following form:

$$s_u = \begin{cases} 0, & \text{in } \Omega_1 \\ 0, & \text{in } \Omega_2 \\ s_{u_3}, & \text{in } \Omega_3. \end{cases}$$

Fick's law states that a substance's diffusive flux is proportional to the gradient of the substance's concentration. This means that a normally distributed substance would be diffused equally in every spatial direction. This does not seem to apply to epithelial cells, which are distributed across the vaginal epithelium. The superficial cells exfoliate continuously, while the basal cells move toward the surface and replace them.[43] Therefore, we assume that a modified Fick's law governs the movement of epithelial cells, with their diffusive flux being equal to

$$\boldsymbol{D_u} \odot \nabla u,$$

with $\odot$ being the Hadamard product and

$$\boldsymbol{D_u} = (D_{u_{xy}}, D_{u_{xy}}, D_{u_z})$$

being the collective diffusion coefficient of u, with $D_{u_{xy}} < D_{u_z}$. Therefore, the diffusion term for the concentration of epithelial cells is equal to

$$\nabla \cdot [\boldsymbol{D_u} \odot \nabla u].$$

This term, instead of describing random motility like a diffusion described by Fick's law would, describes a type of weighted random motility, with a skew toward faster movement on the z-axis.

In addition, we assume that epithelium cells decay exponentially, and at a faster rate when in Ω_1, due to the lack of nutrients. Therefore, we have that the term $-m_u(\mathbf{x})u$ models the exponential decay of epithelial cells, with the rate of exponential decay of u being:

$$m_u = \begin{cases} m_{u_1}, & \text{in } \Omega_1, \\ m_{u_2}, & \text{in } \Omega_2, \\ m_{u_3}, & \text{in } \Omega_3, \end{cases}$$

where $m_{u_1} < \min(m_{u_2}, m_{u_3})$.

We assume that virus particles mutate epithelial cells into dysplastic cells with a constant rate. We model this mutation with the term $-kvu$, with k being the rate of mutation and the negative sign indicating that epithelial cells are lost during this procedure.

Furthermore, we assume zero flux boundary conditions. Thus,

$$\frac{\partial u}{\partial n} = 0, \quad \text{on } \partial\Omega.$$

The initial condition of the epithelium cells, u_∞, is to be extracted as follows. Using the finite element software analysis COMSOL Multiphysics® 6.1,[49] we numerically solve, until a time point, the following problem:

$$\begin{aligned} \frac{\partial u}{\partial t} &= \nabla \cdot [\boldsymbol{D_u} \odot \nabla u] + s_u - m_u u - k v u, && \text{in } \Omega^\circ, \\ \frac{\partial u}{\partial n} &= 0, && \text{on } \partial\Omega, \\ u(\cdot, 0) &= 0, && \text{in } \Omega. \end{aligned}$$

For each f, its solution seems to be converging toward an equilibrium, which we consider to be u_∞. In this way, we initialize the distribution of epithelial cells across Ω before any pathological interaction takes place.

Summing up, we have that

$$\begin{aligned} \frac{\partial u}{\partial t} &= \nabla \cdot [\boldsymbol{D_u} \odot \nabla u] + s_u - m_u u - k v u, && \text{in } \Omega^\circ, \\ \frac{\partial u}{\partial n} &= 0, && \text{on } \partial\Omega, \\ u(\cdot, 0) &= u_\infty, && \text{in } \Omega. \end{aligned}$$

2.2.2 | Viral particles

HPV infection is initiated when the virus comes into contact with the basal epithelial cells, which are typically reached through a microabrasion in the epithelial tissue.[50–52] The initial contact between the epithelium and the viral particles happens at the superficial epithelium. In addition, the frequency of sexual intercourse or other intimate skin-to-skin contact is a risk factor.[53] Therefore, in order to capture the above key mechanisms, we assume that there is a spatially small, time-dependent constant source of HPV viral particles at the superficial epithelium. We write that source at point $(\mathbf{x}, t) \in \Omega \times \mathbb{R}_{\geq 0}$ as $s_v(\mathbf{x}, t)$.

Consequently, we assume that the aforementioned movement of viral particles from the superficial epithelium to the basal layer happens in two ways. The first one is through random motility in space, so we model it using the diffusion term $D_v \Delta v$, with D_v being the diffusion coefficient of v. The second one is through a directed movement toward the epithelial cells, therefore we model it using the advection term $-a_v \nabla \cdot \left[\tau_v \frac{v}{v+b} \nabla u\right]$, with τ_v being the velocity field coefficient of v toward u, and b being the v value for half-maximal velocity of v toward u. We choose the velocity field of the viral particles to be a Michaelis–Menten function.

In addition, we assume that the HPV viral particles decay exponentially. Hence, we introduce the term $-m_v v$, with m_v being the rate of exponential decay of v.

Furthermore, the number of HPV viral particles may increase in dysplastic epithelial cells due to the uncontrollable expression of HPV oncogenes, leading to the maintenance of the transformed phenotype and ultimately promoting the development of cancer.[52] Thus, we assume that dysplastic cells increase the concentration of viral particles. To model this, we introduce the

nonlinear logistic term

$$r_v v\left(pc - \frac{v}{q}\right),$$

where r_v is the growth rate of v, q is a carrying-capacity-like quantity for v, and p is an inverse-carrying-capacity-like quantity for v. We note that q and p have the same and the inverse dimensions, respectively, as the carrying capacity of the common logistic term. For $c \neq 0$, we notice that the above term is equal to $r_v pcv\left(1 - \frac{v}{pqc}\right)$. In this form, it is clear that the carrying capacity and the growth rate of the concentration of HPV viral particles is proportional to the concentration of dysplastic cells.

Finally, we assume zero flux boundary conditions and an initial condition equal to zero.

Summing up, we have that

$$\begin{aligned}
\frac{\partial v}{\partial t} &= D_v \Delta v - a_v \nabla \cdot \left[\tau_v \frac{v}{v+b} \nabla u\right] + s_v - m_v v + r_v v\left(pc - \frac{v}{q}\right), && \text{in } \Omega^\circ,\\
\frac{\partial v}{\partial n} &= 0, && \text{on } \partial\Omega,\\
v(\cdot, 0) &= 0, && \text{in } \Omega.
\end{aligned}$$

2.2.3 | Dysplastic cells

Regarding the movement of dysplastic cells, we employ the same idea as the one we used for the epithelial cells with a weighted random motility type of movement. Thus, we have that the diffusion term for the dysplastic cells is

$$\nabla \cdot [\boldsymbol{D_c} \odot \nabla c],$$

with $\boldsymbol{D_c}$ being the collective diffusion coefficient of c.

Furthermore, we assume that in $\Omega_2 \cup \Omega_3$, without immune response, neoplastic cells do not decay.[54] However, we assume that in Ω_1 they decay exponentially, due to the lack of nutrients. Therefore, we have that the term $-m_c(\mathbf{x})u$ models the exponential decay of epithelial cells, with

$$m_c(\mathbf{x}) = \begin{cases} m_{c_1}, & \text{in } \Omega_1,\\ 0, & \text{otherwise,} \end{cases}$$

being the rate of exponential decay of c.

As we discussed for the case of HPV virus particles, we assume that the epithelial cells mutate into dysplastic cells with a rate of kvu. The term's positive sign indicates that the concentration of dysplastic cells increases during this procedure.

Moreover, we assume that immune cells kill dysplastic cells with a Holling type I functional response. Hence, we have that the term describing this procedure is $-dwc$, with d being the rate of w-induced c death.

Finally, we assume zero flux boundary conditions and an initial condition equal to zero.

Summing up, we have that

$$\begin{aligned}
\frac{\partial c}{\partial t} &= \nabla \cdot [\boldsymbol{D_c} \odot \nabla c] - m_c c + k v u - d w c, && \text{in } \Omega^\circ, \\
\frac{\partial c}{\partial n} &= 0, && \text{on } \partial\Omega, \\
c(\cdot, 0) &= 0, && \text{in } \Omega.
\end{aligned}$$

2.2.4 | Immune cells

Different types of immune cells, such as leukocytes, neutrophils, and monocytes, preferentially migrate through areas of the basement membrane that have lower protein deposition, such as laminin and collagen IV. These cells can migrate through existing openings in the basement membrane. For instance, monocytes are highly deformable and can squeeze through these openings, while neutrophils can lead to remodeling and enlargement of these sites. Dendritic cells, another type of immune cell, have been shown to migrate through preexisting openings in the lymphatic basement membrane by widening these small gaps. After these gaps are widened by cells, they return to a baseline slightly larger than the original gap size, indicating the mechanical plasticity of the basement membrane.[55] Therefore, we assume that the greater the concentration of dysplastic cells near the basement membrane, the higher the influx of immune cells that pass through it. Hence, we have that

$$\frac{\partial w}{\partial n} = jc, \quad \text{on } \mathrm{gr} f,$$

where j is the flux coefficient through the basement membrane, and

$$\mathrm{gr} f = \left\{(x, y, z) \in [0, L_x] \times [0, L_y] \times [\min f, L_z] | z = f(x, y)\right\}$$

stands for the graph of f.

Regarding the movement of immune cells, we assume that immune cells move both in a random and in a directed way. The random movement of immune cells is modeled by the diffusion term $D_w \Delta w$, with D_w being the diffusion coefficient of w. On the other hand, the directed movement of immune cells toward dysplastic cells is modeled by the advection term $-a_w \nabla \cdot [\tau_w w \nabla c]$, with a_w being the advection coefficient of w, and τ_w being the velocity field coefficient of w toward c.

Moreover, we assume that the immune cells decay exponentially. Hence, we introduce the term $-m_w w$, with m_w being the rate of exponential decay of w.

Finally, we have that the initial concentration of immune cells is equal to zero.

Summing up, we have that

$$\begin{aligned}
\frac{\partial w}{\partial t} &= D_w \Delta w - a_w \nabla \cdot [\tau_w w \nabla c] - m_w w, && \text{in } \Omega^\circ, \\
\frac{\partial w}{\partial n} &= jc, && \text{on } \mathrm{gr} f,
\end{aligned}$$

$$\frac{\partial w}{\partial n} = 0, \qquad \text{on } \partial\Omega \setminus \mathrm{gr} f,$$
$$w(\cdot, 0) = 0, \qquad \text{in } \Omega.$$

2.3 | The integrated model

Integrating the histological and the pathological part of the model presented in Sections 2.1 and 2.2, respectively, we arrive at the initial-boundary-value problem that describes the problem in question.

Our model consists of the following system of nonlinear reaction–diffusion–advection equations

$$\frac{\partial u}{\partial t} = \nabla \cdot [\boldsymbol{D_u} \odot \nabla u] + s_u - m_u u - k v u, \tag{6a}$$

$$\frac{\partial v}{\partial t} = D_v \Delta v - a_v \nabla \cdot \left[\tau_v \frac{v}{v+b} \nabla u\right] + s_v - m_v v + r_v v \left(pc - \frac{v}{q}\right), \tag{6b}$$

$$\frac{\partial c}{\partial t} = \nabla \cdot [\boldsymbol{D_c} \odot \nabla c] - m_c c + k v u - d w c, \tag{6c}$$

$$\frac{\partial w}{\partial t} = D_w \Delta w - a_w \nabla \cdot [\tau_w w \nabla c] - m_w w \tag{6d}$$

in Ω°, with initial conditions

$$u(\cdot, 0) = u_\infty,$$
$$v(\cdot, 0) = 0,$$
$$c(\cdot, 0) = 0,$$
$$w(\cdot, 0) = 0$$

in Ω, along with boundary conditions

$$\frac{\partial u}{\partial n} = \frac{\partial v}{\partial n} = \frac{\partial c}{\partial n} = 0, \qquad \text{on } \partial\Omega,$$
$$\frac{\partial w}{\partial n} = 0, \qquad \text{on } \partial\Omega \setminus \mathrm{gr} f,$$
$$\frac{\partial w}{\partial n} = jc, \qquad \text{on } \mathrm{gr} f.$$

Tables 1 and 2 list the terms, as well as the variables and parameters, respectively, of our model, along with a brief description. In Table 3, we present scales of the variables and estimations of the parameters, which will be used later on during the numerical simulations.

Finally, we note that by utilizing common techniques of nondimensionalization, we can eliminate only three of the 32 parameters in total.

TABLE 1 Description of the terms of the model.

Deriv.	Term	Description
$\frac{\partial u}{\partial t}$	$\nabla \cdot [\boldsymbol{D_u} \odot \nabla u]$	Weighted random motility of epithelial cells
	s_u	Constant source of epithelial cells
	$-m_u u$	Exponential decay of epithelial cells
	$-kvu$	Mutation of epithelial cells to dysplastic cells due to viral particles
$\frac{\partial v}{\partial t}$	$D_v \Delta v$	Random motility of viral particles
	$-a_v \nabla \cdot \left[\tau_v \frac{v}{v+b} \nabla u\right]$	Directed movement of viral particles toward epithelial cells
	s_v	Constant source of viral particles
	$-m_v v$	Exponential decay of viral particles
	$r_v v \left(pc - \frac{v}{q}\right)$	Logistic growth of viral particles
$\frac{\partial c}{\partial t}$	$\nabla \cdot [\boldsymbol{D_c} \odot \nabla c]$	Weighted random motility of dysplastic cells
	$-m_c c$	Exponential decay of dysplastic cells
	kvu	Mutation of epithelial cells to dysplastic cells due to viral particles
	$-dwc$	Immune-cell-induced dysplastic cell death
$\frac{\partial w}{\partial t}$	$D_w \Delta w$	Random motility of immune cells
	$-a_w \nabla \cdot [\tau_w w \nabla c]$	Directed movement of immune cells toward dysplastic cells
	$-m_w w$	Exponential decay of immune cells

3 | DYSPLASIA PROGRESSION: THREE KEY FACTORS

In the present section, we numerically solve the proposed problem, in order to highlight the importance of the shape of the basement membrane, the strength of the immune response, and the frequency of viral exposure. All numerical simulations are carried out using the finite element analysis software COMSOL Multiphysics 6.1.

The values of the parameters are as in Table 3, unless otherwise noted. In order to incorporate the effect of the exposure to HPV, we assume that $s_v \neq 0$, in particular

$$s_v = \begin{cases} 6.40 \cdot 10^{-2}\ \mu\text{m}^3\,\text{d}^{-1}, & \text{in } \Omega_{1_s} \times T_s, \\ 0, & \text{otherwise} \end{cases}$$

for

$$\Omega_{1_s} = \left[4.50 \cdot 10^1, 5.50 \cdot 10^1\right]^2 \times \left[9.00 \cdot 10^1, 1.00 \cdot 10^2\right]\ \mu\text{m}^3 \subsetneq \Omega_1$$

and for some $T_s \subsetneq \mathbb{R}_{\geq 0}$ which is left to be chosen. T_s is the union of half-hour intervals, with each one representing a sexual encounter with an HPV positive partner.[57]

3.1 | Basement membrane's shape

Here, assuming that $T_s = \left[2, 2 + \frac{1}{48}\right]$ d and $j = 0$, we only vary the geometrical characteristics of the model. Therefore, drawing samples from ℓ and ϕ, while keeping the rest of the parameters

TABLE 2 Description of the independent and dependent variables as well as parameters of the model, along with their units.

	Name	Description	Physical dimension
Independent variables	x	Length	L
	y	Length	L
	z	Length	L
	t	Time	T
Dependent variables	u	Concentration of epithelial cells	$\#\,L^{-3}$
	v	Concentration of viral particles	$\#\,L^{-3}$
	c	Concentration of dysplastic cells	$\#\,L^{-3}$
	w	Concentration of immune cells	$\#\,L^{-3}$
Parameters	$\boldsymbol{D_u}$	Collective diffusion coefficient of u	$L^2\,T^{-1}$
	s_u	Constant source of u	$\#\,L^{-3}\,T^{-1}$
	m_u	Rate of exponential decay of u	T^{-1}
	k	Rate of mutation of u to c	$\#^{-1}\,L^3\,T^{-1}$
	D_v	Diffusion coefficient of v	$L^2\,T^{-1}$
	a_v	Advection coefficient of v	L^2
	τ_v	Velocity field coefficient of v toward u	T^{-1}
	b	v value for half-maximal velocity of v toward u	$\#\,L^{-3}$
	s_v	Constant source of v	$\#\,L^{-3}\,T^{-1}$
	m_v	Rate of exponential decay of v	T^{-1}
	r_v	Growth rate of v	T^{-1}
	p	Inverse-carrying-capacity-like quantity of v	$\#^{-1}\,L^3$
	q	Carrying-capacity-like quantity of v	$\#\,L^{-3}$
	$\boldsymbol{D_c}$	Collective diffusion coefficient of c	$L^2\,T^{-1}$
	m_c	Rate of exponential decay of c	T^{-1}
	d	Rate of w-induced c death	$\#^{-1}\,L^3\,T^{-1}$
	D_w	Diffusion coefficient of w	$L^2\,T^{-1}$
	a_w	Advection coefficient of w	L^2
	τ_w	Velocity field coefficient of w toward c	$\#^{-1}\,L^3\,T^{-1}$
	m_w	Rate of exponential decay of w	T^{-1}
	j	Flux coefficient through the basement membrane	L^{-1}
	L_x	Length of Ω in x-axis	L
	L_y	Length of Ω in y-axis	L
	L_z	Lowest admissible value of the length of Ω in z-axis	L
	ℓ	Amplitude coefficient	L
	ϕ	Phase angle	L
	β	Spectral exponent	–
	h	Width of the basal layer	L

TABLE 3 Scales of the variables and estimated parameter values of the model. The value of the ratio $\frac{h}{L_z} \approx 30\%$ is taken from Ref. 56, whereas the value of L_z is taken from Ref. 46. The rest of the parameters are estimated.

	Name	Value	Unit
Scales	x_0	$1.00 \cdot 10^2$	μm
	y_0	$1.00 \cdot 10^2$	μm
	z_0	$1.00 \cdot 10^2$	μm
	t_0	1.00	d
	u_0	2.64	$\# \mu m^{-3}$
	v_0	$2.70 \cdot 10^1$	$\# \mu m^{-3}$
	c_0	$2.70 \cdot 10^1$	$\# \mu m^{-3}$
	w_0	$4.30 \cdot 10^{-2}$	$\# \mu m^{-3}$
Parameters	$\boldsymbol{D_u}$	$\left(8.16 \cdot 10^2, 8.16 \cdot 10^2, 2.94 \cdot 10^4\right)$	$\mu m^2\, d^{-1}$
	s_{u_3}	$2.10 \cdot 10^{-1}$	$\# \mu m^{-3}\, d^{-1}$
	m_{u_1}	$8.00 \cdot 10^{-1}$	d^{-1}
	m_{u_2}	$5.00 \cdot 10^{-2}$	d^{-1}
	m_{u_3}	$5.00 \cdot 10^{-2}$	d^{-1}
	k	$1.40 \cdot 10^1$	$\#^{-1}\, \mu m^3\, d^{-1}$
	D_v	$4.90 \cdot 10^4$	$\mu m^2\, d^{-1}$
	a_v	$1.04 \cdot 10^4$	μm^2
	τ_v	1.00	d^{-1}
	b	$2.10 \cdot 10^{-2}$	$\# \mu m^{-3}$
	s_v	varied	$\# \mu m^{-3}\, d^{-1}$
	m_v	$9.00 \cdot 10^{-4}$	d^{-1}
	r_v	$1.00 \cdot 10^{-3}$	d^{-1}
	p	$2.33 \cdot 10^1$	$\#^{-1}\, \mu m^3$
	q	$2.33 \cdot 10^1$	$\#^{-1}\, \mu m^3$
	q	$0.43 \cdot 10^{-1}$	$\#^{-1}\, \mu m^{-3}$
	$\boldsymbol{D_c}$	$\left(8.16 \cdot 10^2, 8.16 \cdot 10^2, 1.22 \cdot 10^5\right)$	$\mu m^2\, d^{-1}$
	m_{c_1}	$8.00 \cdot 10^{-1}$	d^{-1}
	d	$2.33 \cdot 10^1$	$\#^{-1}\, \mu m^3\, d^{-1}$
	D_w	$4.90 \cdot 10^4$	$\mu m^2\, d^{-1}$
	a_w	$8.20 \cdot 10^{-2}$	μm^2
	τ_w	$2.33 \cdot 10^1$	$\#^{-1}\, \mu m^3\, d^{-1}$
	m_w	$1.00 \cdot 10^{-2}$	d^{-1}
	j	varied	μm^{-1}
	L_x	$1.00 \cdot 10^2$	μm
	L_y	$1.00 \cdot 10^2$	μm
	L_z	$1.00 \cdot 10^2$	μm
	ℓ	$\mathcal{N}_2(\mathbf{0}_2, \boldsymbol{I}_2)$	μm
	ϕ	$\mathcal{U}\left(\left[-\frac{\pi}{2}, \frac{\pi}{2}\right]^2\right)$	μm
	β	6.50	–
	h	$3.00 \cdot 10^1$	μm

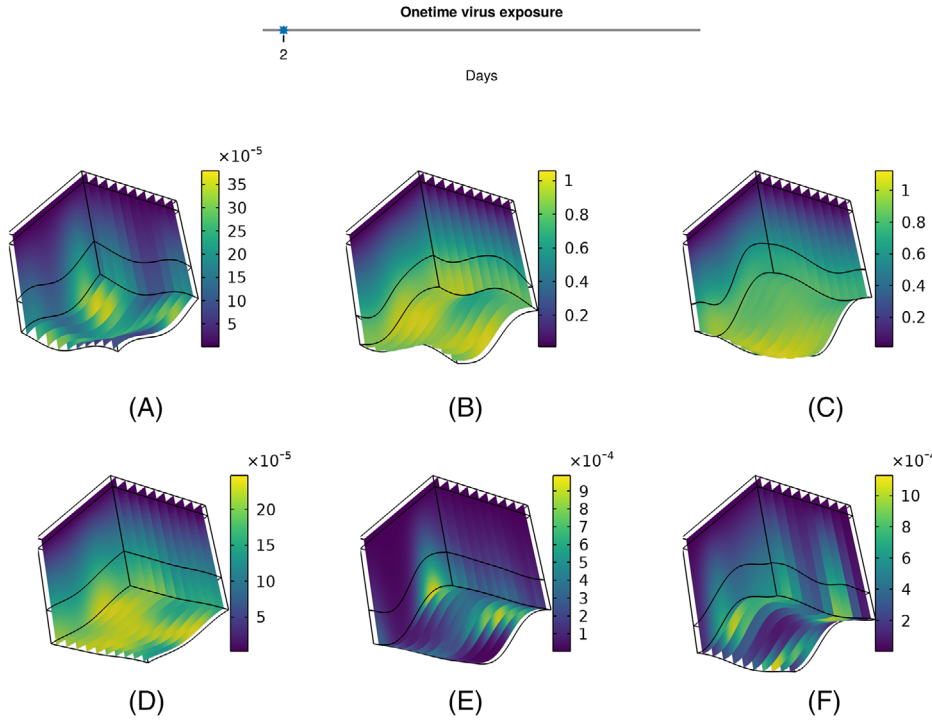

FIGURE 5 Dysplastic cells after 3600 days. The geometry of the basement membrane varies between each simulation, while keeping the rest of the parameters fixed. We observe that this factor alone shapes the outcome of the infection. Namely, in simulations (A) and (D–F) the dysplastic cells tend to vanish, while in (B) and (C) they are established.

fixed, we arrive at Figure 5. We notice that in some cases dysplastic cells vanish, whereas in others they persist. Hence, the ability of dysplastic cells to establish themselves is strongly dependent on the shape of the basement membrane.

3.2 | Immune response's strength

Assuming that $T_S = \left[2, 2 + \frac{1}{48}\right]$ d and f is fixed, while only varying the value of j, we arrive at Figure 6. We deduce that as j decreases, the establishment of dysplastic cells is facilitated.

3.3 | Viral exposure's frequency

Assuming that $j = 3.86 \cdot 10^1\ \mu\text{m}^{-1}$ and f is fixed, while only varying T_s, we arrive at Figures 7, 8, and 9. We observe that the frequency of viral exposure determines the presence of dysplastic cells and increases the rate of their establishment. Therefore, this frequency has both qualitative and quantitative effect on the ultimate presence of precancerous lesions.

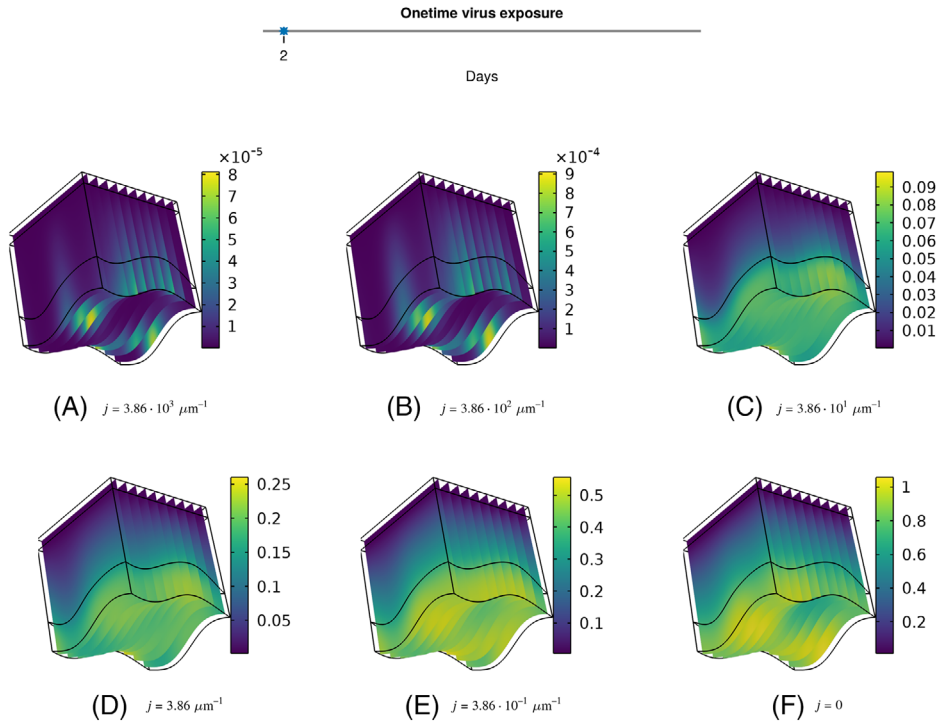

FIGURE 6 Dysplastic cells after 3600 days. j varies between each simulation, while keeping the rest of the parameters fixed. We observe the qualitative change of the outcome as j varies between $3.86 \cdot 10^2$ and $3.86 \cdot 10^1\ \mu m^{-1}$.

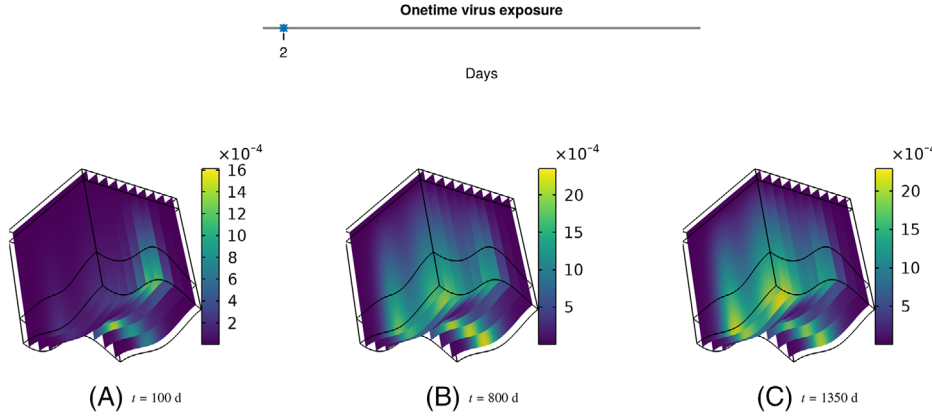

FIGURE 7 Snapshots of dysplastic cells for three different days. Here, $T_s = \left[2, 2 + \frac{1}{48}\right]$ d. We observe that a onetime virus exposure is unable to cause dysplastic cell establishment, for this particular parameter set.

4 | CONCLUSION AND DISCUSSION

In this paper, we introduced a model of nonlinear partial differential equations describing the dynamics of epithelial cells, viral particles, dysplastic cells, and immune cells. The model was

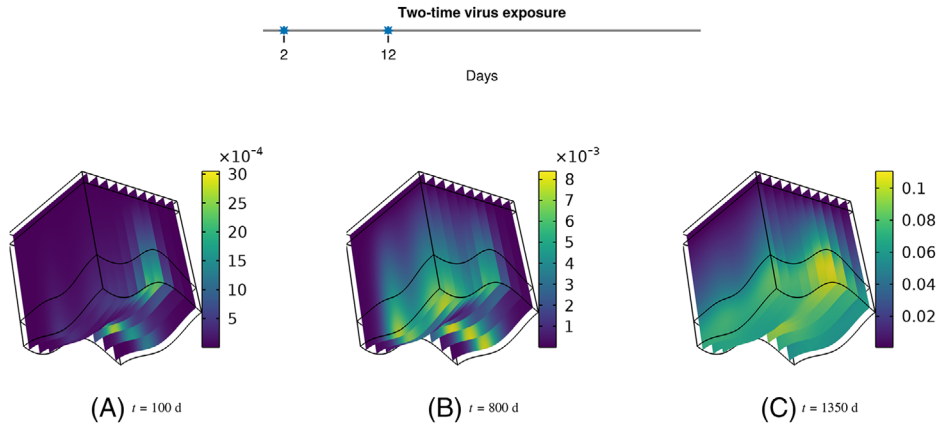

FIGURE 8 Snapshots of dysplastic cells for three different days. Here, $T_s = \left[2, 2 + \frac{1}{48}\right] \cup \left[12, 12 + \frac{1}{48}\right]$ d. We observe that, contrary to a onetime virus exposure, a two-time exposure is able to cause dysplastic cell establishment, for the same parameter set.

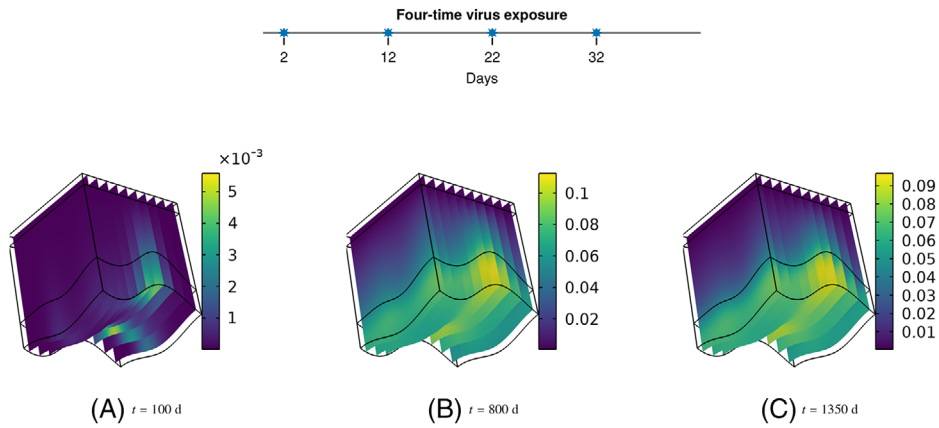

FIGURE 9 Snapshots of dysplastic cells for three different days. Here, $T_s = \bigcup_{i \in \{2,12,22,32\}} \left[i, i + \frac{1}{48}\right]$ d. We observe that a four-time virus exposure speeds up the establishment of dysplastic cells when compared to a two-time exposure, for the same parameter set.

then used to numerically investigate the key characteristics of dysplasia progression. From this investigation, we deduced that

- the shape of the basement membrane alone can dictate the ability of dysplastic cells to establish themselves in the epithelium
- the smaller the flux of immune cells through the basement membrane, the greater the concentration of dysplastic cells
- the frequency of the viral exposure determines both the existence of dysplastic cells and the speed of their aggregation.

Our work can be extended from both an analytical and a modeling point of view. Concerning the analytical perspective, we plan to study the model in terms of global well-posedness and stability

analysis. Moreover, we intend to explicitly determine the dependence of the solution on the geometrical data of the membrane, the flux of immune cells, as well as the source of the viral exposure.

As for the modeling perspective, we could extend this study by extracting a condition for the prediction of the compliant/critical points of the basement membrane that would cause the transition from the CIS to cancer. In addition, we plan to extensively study the role of different immune cells, instead of grouping them together into one variable. Moreover, a straightforward generalization includes the consideration of infection with different strains of HPV. Finally, we plan to incorporate a new dependent variable that will model the level of mutation of epithelial cells.

ACKNOWLEDGMENTS

The authors would like to thank Stratis Manifavas for his comments on random variables used in Section 2.1.1.

FUNDING INFORMATION

The publication of the article in OA mode was financially supported by HEAL-Link.

DATA AVAILABILITY STATEMENT

The data that support the findings of this study are available from the corresponding author upon reasonable request.

ORCID

Vasiliki Bitsouni https://orcid.org/0000-0002-0684-0583
Nikolaos Gialelis https://orcid.org/0000-0002-6465-7242
Ioannis G. Stratis https://orcid.org/0000-0002-0179-0820
Vasilis Tsilidis https://orcid.org/0000-0001-5868-4984

REFERENCES

1. Hanahan D, Weinberg RA. The hallmarks of cancer. *Cell*. 2000;100(1):57-70.
2. Marusyk A, Almendro V, Polyak K. Intra-tumour heterogeneity: a looking glass for cancer? *Nat Rev Cancer*. 2012;12(5):323-334.
3. Méndez-López LF. Revisiting epithelial carcinogenesis. *Int J Mol Sci*. 2022;23(13):7437.
4. Ogino S, Galon J, Fuchs CS, Dranoff G. Cancer immunology—analysis of host and tumor factors for personalized medicine. *Nat Rev Clin Oncol*. 2011;8(12):711-719.
5. World Health Organization. Cervical cancer. 2023. https://www.who.int/news-room/fact-sheets/detail/cervical-cancer
6. Sung H, Ferlay J, Siegel RL, et al. Global cancer statistics 2020: GLOBOCAN estimates of incidence and mortality worldwide for 36 cancers in 185 countries. *CA Cancer J Clin*. 2021;71(3):209-249.
7. DeMay RM. *Practical Principles of Cytopathology*. American Society of Clinical Pathologists Press; 1999.
8. Santesso N, Mustafa RA, Schünemann HJ, et al. World Health Organization guidelines for treatment of cervical intraepithelial neoplasia 2–3 and screen-and-treat strategies to prevent cervical cancer. *Int J Gynecol Obstet*. 2016;132(3):252-258.
9. Salcedo MP, Phoolcharoen N, Schmeler KM. Intraepithelial neoplasia of the lower genital tract (cervix, vagina, vulva): etiology, screening, diagnosis, management. In: *Comprehensive Gynecology*. Elsevier; 2021:637.
10. World Health Organization. Histopathology of the uterine cervix - digital atlas: WHO histological classification of tumours of the uterine cervix. https://screening.iarc.fr/atlasclassifwho.php
11. Schiffman M, Castle PE, Jeronimo J, Rodriguez AC, Wacholder S. Human papillomavirus and cervical cancer. *Lancet*. 2007;370(9590):890-907.
12. Guan P, Howell-Jones R, Li N, et al. Human papillomavirus types in 115,789 HPV-positive women: a meta-analysis from cervical infection to cancer. *Int J Cancer*. 2012;131(10):2349-2359.

13. The Cancer Genome Atlas Research Network. Integrated genomic and molecular characterization of cervical cancer. *Nature*. 2017;543:378-384.
14. Kusakabe M, Taguchi A, Sone K, Mori M, Osuga Y. Carcinogenesis and management of human papillomavirus-associated cervical cancer. *Int J Clin Oncol*. 2023;28:965-974.
15. Bzhalava D, Guan P, Franceschi S, Dillner J, Clifford G. A systematic review of the prevalence of mucosal and cutaneous human papillomavirus types. *Virology*. 2013;445(1-2):224-231.
16. Tommasino M. The human papillomavirus family and its role in carcinogenesis. *Semin Cancer Biol*. 2014;26:13-21.
17. Ljubojevic S, Skerlev M. HPV-associated diseases. *Clin Dermatol*. 2014;32(2):227-234.
18. National Cancer Institute. HPV and Cancer. March 1, 2019. Retrieved April 27, 2023. https://www.cancer.gov/about-cancer/causes-prevention/risk/infectious-agents/hpv-and-cancer
19. Perkins RB, Wentzensen N, Guido RS, Schiffman M. Cervical cancer screening: a review. *JAMA*. 2023;330(6):547-558.
20. Walboomers JMM, Jacobs MV, Manos MM, et al. Human papillomavirus is a necessary cause of invasive cervical cancer worldwide. *J Pathol*. 1999;189(1):12-19.
21. Moody CA, Laimins LA. Human papillomavirus oncoproteins: pathways to transformation. *Nat Rev Cancer*. 2010;10(8):550-560.
22. Doorbar J, Egawa N, Griffin H, Kranjec C, Murakami I. Human papillomavirus molecular biology and disease association. *Rev Med Virol*. 2015;25:2-23.
23. Stubenrauch F, Laimins LA. Human papillomavirus life cycle: active and latent phases. *Semin Cancer Biol*. 1999;9:379-386.
24. Keiffer TR, Soorya S, Sapp MJ. Recent advances in our understanding of the infectious entry pathway of human papillomavirus type 16. *Microorganisms*. 2021;9(10):2076.
25. Asih TSN, Lenhart S, Wise S, et al. The dynamics of HPV infection and cervical cancer cells. *Bull Math Biol*. 2016;78:4-20.
26. Lee C, Laimins LA. The differentiation-dependent life cycle of human papillomaviruses in keratinocytes. In: *The Papillomaviruses*. Springer; 2007:45-67.
27. World Health Organization. Reaching 2030 cervical cancer elimination targets—new WHO recommendations for screening and treatment of cervical pre-cancer. 2021. https://www.who.int/news-room/events/detail/2021/07/06/default-calendar/reaching-2030-cervical-cancer-elimination-targets
28. World Health Organization–Organisation mondiale de la Santé. Human papillomavirus vaccines: WHO position paper (2022 update)–Vaccins contre les papillomavirus humains: note de synthèse de l' OMS (mise à jour de 2022). *Wkly Epidemiol Rec*. 2022;97(50):645-672.
29. World Health Organization. Human papillomavirus vaccines (HPV). 2022. https://www.who.int/teams/immunization-vaccines-and-biologicals/diseases/human-papillomavirus-vaccines-(HPV)
30. Solis FJ, Gonzalez LM. A numerical approach for a model of the precancer lesions caused by the human papillomavirus. *J Differ Equ Appl*. 2017;23(6):1093-1104.
31. Solis FJ, Gonzalez LM. A nonlinear transport–diffusion model for the interactions between immune system cells and HPV-infected cells. *Nonlinear Dyn*. 2023:1-15.
32. Barnabas RV, Laukkanen P, Koskela P, Kontula O, Lehtinen M, Garnett GP. Epidemiology of HPV 16 and cervical cancer in Finland and the potential impact of vaccination: mathematical modelling analyses. *PLoS Med*. 2006;3(5):e138.
33. Elbasha EH. Global stability of equilibria in a two-sex HPV vaccination model. *Bull Math Biol*. 2008;70:894-909.
34. Brown V, White KAJ. The HPV vaccination strategy: could male vaccination have a significant impact? *Comput Math Methods Med*. 2010;11(3):223-237.
35. Brown VL, White KAJ. The role of optimal control in assessing the most cost-effective implementation of a vaccination programme: HPV as a case study. *Math Biosci*. 2011;231(2):126-134.
36. Lee SL, Tameru AM. A mathematical model of human papillomavirus (HPV) in the United States and its impact on cervical cancer. *J Cancer*. 2012;3:262-268.
37. Sado AE. Mathematical modeling of cervical cancer with HPV transmission and vaccination. *Scie J Appl Math Stat*. 2019;7(2):21-25.
38. Gurmu ED, Bole BK, Koya PR. Mathematical model for co-infection of HPV with cervical cancer and HIV with AIDS diseases. *Int J Sci Res Math Stat Sci*. 2020;7(2):107-121.

39. Rajan PK, Kuppusamy M, Egbelowo OF. A mathematical model for human papillomavirus and its impact on cervical cancer in India. *J Appl Math Comput*. 2023;69(1):753-770.
40. Chakraborty S, Cao X, Bhattyacharya S, Roy PK. The role of HPV on cervical cancer with several functional response: a control based comparative study. *Comput Math Model*. 2019;30:439-453.
41. Prendiville W, Sankaranarayanan R. *Colposcopy and Treatment of Cervical Precancer*. International Agency for Research on Cancer, World Health Organization; 2017.
42. Pastar I, Stojadinovic O, Yin NC, et al. Epithelialization in wound healing: a comprehensive review. *Adv Wound Care*. 2014;3(7):445-464.
43. Kierszenbaum AL, Tres L. *Histology and Cell Biology: An Introduction to Pathology E-Book*. Elsevier Health Sciences; 2015.
44. Pozzi A, Yurchenco PD, Iozzo RV. The nature and biology of basement membranes. *Matrix Biol*. 2017;57:1-11.
45. Kurman RJ. *Blaustein's Pathology of the Female Genital Tract*. Springer Science & Business Media; 2013.
46. Mescher AL. *Junqueira's Basic Histology: Text and Atlas*. McGraw Hill; 2018.
47. Barnsley MF, Devaney RL, Mandelbrot BB, et al. *The Science of Fractal Images*. Vol 1. Springer; 1988.
48. Sjodin B. How to generate random surfaces in COMSOL Multiphysics®. *Comsol Blog*. 2017.
49. COMSOL AB. COMSOL Multiphysics. https://comsol.com
50. Münger K, Baldwin A, Edwards KM, et al. Mechanisms of human papillomavirus-induced oncogenesis. *J Virol*. 2004;78(21):11451-11460.
51. Schiller JT, Day PM, Kines RC. Current understanding of the mechanism of HPV infection. *Gynecol Oncol*. 2010;118(1):S12-S17.
52. Pešut E, Đukić A, Lulić L, et al. Human papillomaviruses-associated cancers: an update of current knowledge. *Viruses*. 2021;13(11):2234.
53. Veldhuijzen NJ, Snijders PJF, Reiss P, Meijer CJLM, van de Wijgert JH. Factors affecting transmission of mucosal human papillomavirus. *Lancet Infect Dis*. 2010;10(12):862-874.
54. Park WY, Gray JM, Holewinski RJ, et al. Apoptosis-induced nuclear expulsion in tumor cells drives S100a4-mediated metastatic outgrowth through the RAGE pathway. *Nat Cancer*. 2023;4(3):419-435.
55. Chang J, Chaudhuri O. Beyond proteases: basement membrane mechanics and cancer invasion. *J Cell Biol*. 2019;218(8):2456-2469.
56. Chandrasoma PT. *GERD: A New Understanding of Pathology, Pathophysiology, and Treatment*. Academic Press; 2017.
57. Blair KL, Pukall CF. Can less be more? Comparing duration vs. frequency of sexual encounters in same-sex and mixed-sex relationships. *Can J Hum Sex*. 2014;23(2):123-136.

How to cite this article: Bitsouni V, Gialelis N, Stratis IG, Tsilidis V. From primary HPV infection to carcinoma in situ: A mathematical approach to cervical intraepithelial neoplasia. *Stud Appl Math*. 2024;153:e12697. https://doi.org/10.1111/sapm.12697